*Desalination and Water Treatment*
www.deswater.com

doi:10.5004/dwt.2018.22942

131 (2018) 291–304
November

# Adsorption of hexavalent chromium by crushed brick: effect of operating parameters and modeling study

Assia Allaoui[a], Zhour Hattab[a,*], Radia Zerdoum[b], Ridha Djellabi[a], Yamina Berredjem[b], Wahiba Bessashia[b], Kamel Guerfi[a]

[a]*Laboratory of Water Treatment and Valorization of Industrial Wastes, Department of Chemistry, Faculty of Sciences, Badji-Mokhtar University, B.P.12, Annaba 23000, Algeria, email: assia_lazi@yahoo.fr (A. Allaoui), Tel. +213540971723, email: zoumourouda20012000@yahoo.fr (Z. Hattab), ridha.djellabi@yahoo.com (R. Djellabi), k_guerfi@yahoo.fr (K. Guerfi)*
[b]*Science and Technology Laboratory of Water and Environment,Faculty of Science and Technology, Mohammed Cherif Messadia University, Souk Ahras 41000, Algeria, email: environnement2004@yahoo.fr (R. Zerdoum), y_berredjem@yahoo.fr (Y. Berredjem), bessashiawahiba@yahoo.com (W. Bessashia)*

Received 25 December 2017; Accepted 12 August 2018

**ABSTRACT**

The sorption of hexavalent chromium in aqueous solution using crushed Brick was carried out in batch mode. Powder of crushed Brick was prepared within a size between 500 and 800 µm. The crushed Brick was characterized by Fourier Transform infrared spectra (FTIR), BET surface area, X-ray fluorescence (XRF), Scanning Electron Microscopy (SEM),X-ray diffraction (XRD), Thermogravimetric analysis (TGA)and Zeta Potential. The results showed that the crushed Brick is a typical aluminosilicate mineral with $SiO_2/Al_2O_3$ ratio of 3.65. On the other hand, it has a surface area of 20.11 $m^2 g^{-1}$ and exhibits a net microporosity with a medium pore width of 2.26 Å. Batch experiments were conducted to study the effect of different operating parameters such as contact time, pH, stirring speed, temperature, adsorbent dose and initial Cr(VI) concentration on the adsorption of Cr(VI) by crushed Brick. The results showed that the maximum adsorption capacity was 3.06 mg $g^{-1}$ at pH 3, adsorbent dose of 20 g $L^{-1}$ and initial Cr(VI) concentration of 10 mg $L^{-1}$. Furthermore, the adsorption capacity increases in an acidic medium until it reaches pH 3 and afterwards it decreases due to the different speciation of hexavalent chromium with pH shifting. The equilibrium data were analyzed using three isotherm models such as Langmuir, Freundlich and Temkin by linear method. A satisfactory correlation coefficient value of the Langmuir isotherm demonstrates that the hexavalent chromium adsorption by crushed Brick is monolayer physical adsorption. The kinetic studies showed that the experimental data were best describing by pseudo- second-order model and intra-particle diffusion. It was observed from the values of thermodynamics parameters such as Gibbs free energy (ΔG°), enthalpy (ΔH°), and entropy (ΔS°), that the nature of adsorption is non-spontaneous, exothermic and reflects the decreased randomness at the solid/solution interface during the adsorption.

*Keywords:* Crushed brick; Hexavalentchromium; Adsorption; Modeling; Thermodynamics; Waste valorization

## 1. Introduction

Water is an essential commodity for the survival of all living beings on earth. Therefore, its pollution represents a critical problem for all humanity. Heavy metals present a major source of water pollution that resulted from several industrial activities including metal finishing, textile manufacturing, cement production, chromate production, electroplating, leather tanning and pesticide applications [1,2]. Among these metals, chromium is a common heavy metal contaminant in manufacturing regions. In aquatic environ-

*Corresponding author.

ments, chromium exists in two major forms: Cr(III) and Cr(VI). The last one is more toxic and mobile, and known as human carcinogen and mutagen [3–6]. Due to this, Cr(VI) is in the list of priority water contaminants. The World Health Organization (WHO) prescribed 0.5 mg $g^{-1}$ as a maximum level of Cr(VI) for drinking water [7].

The removal of hexavalent chromium from water has been widely studied by the use of different processes such as electrocoagulation [8], membrane separation [9], chemical precipitation [10], ion exchange [11], nanoparticules [12,13] photocatalysis [14] and adsorption [15]. While the adsorption method is simple, economic and practical for the removal of heavy metals from wastewaters. The fact that commercial activated carbon is of high cost, in recent years numerous researchers have become increasingly interested in the preparation of alternative adsorbents through the exploration of novel industrial solid wastes and natural materials due to their low-cost and their physicochemical properties. Different materials were used as such as Sterculia guttata shell [16]. Ficus auriculata leaves [17] seaweeds [18] Caryotaurens inflorescence [19] Colocasiaesculenta leaves, Annonareticulate, RuelliaPatula Jacq [20] Chitosan [21], Zeolite [22], Bentonite [23], clay or certain industrial waste products like coal [24] fly ash [25], and biomass [26].

In this work crushed Brick, which is an available construction waste, was used as an adsorbent for the removal of Cr(VI) from aqueous solution in batch mode.

The effects of sorbent dose, contact time, stirring speed, initial Cr(VI) concentration, pH and temperature were investigated. The adsorption kinetic data were tested by pseudo-first-order, pseudo-second-order and intra-particle diffusion kinetic models. The equilibrium data were analyzed using three adsorption isotherm models. The thermodynamics of Cr(VI) adsorption and the changes in Gibbs free energy were also evaluated.

## 2. Materials and methods

### 2.1. Chemicals

A stock solution of Cr(VI) 1000 mg $L^{-1}$ was prepared by dissolving a certain amount of potassium dichromate ($K_2Cr_2O_7$) in distilled water and the considered concentrations 5–90 mg $L^{-1}$ were prepared by diluting the stock solution. The residual concentration of Cr(VI) was measured using a UV–Vis spectrophotometer (JENWAL 7315) at a wavelength 540 nm after complexation with 1,5-diphenylcarbazide [27]. Adjustment of the pH of solution was achieved with 0.1 M HCl and 0.1 M NaOH and monitored by a pH meter (HANNA HI9812-5). All products were purchased from Sigma-Aldrich-Fluka (Saint-Quentin, Fallavier, France).

### 2.2. Preparation of crushed Brick adsorbent

The used bricks for this experiment were obtained from local construction company in Annaba (Algeria). Bricks were crushed and sieved to get the particle sizes between 500 and 800 µm. The crushed Brick was washed in water several times and then rinsed in distilled water to remove the impurities. The powder obtained was dried at 110°C and then stored in desiccators until usage.

### 2.3. Characterization of crushed Brick

The chemical analysis of crushed Brick was carried out with X-ray fluorescence (XRF), Fourier transform infrared analysis (FTIR) was recorded to identify the functional groups of crushed Brick material using the IR Affinity-1 in combination with a single reflection ATR. The specific surface area was determined by using $N_2$ as the sorbate at –196°C with an automatic ASAP 2000 apparatus from Micrometrics, the crushed Brick was previously out-gassed at 200°C for 6 h and the specific surface area was determined by the BET method.

Zeta potential measurement of crushed Brick was carried out using a Zetasizer 2000 instrument equipped with a microprocessor at a temperature of 25°C and pH 7. The magnitude of this parameter is often used as a measure of the strength of the attractive/repulsive interactions between particles and to have information about the surface property of the particles in suspension. The XRD patterns of crushed Brick were collected by means of a BRUKER AXS with Cu-K$\alpha_1$(1.54056 Å). Scans were conducted from 0 to 60° at a rate of 2° $min^{-1}$. Thermogravimetric analysis (TGA) was performed using a TGA/DSC 3+ "STAR System" apparatus in order to monitor the mass change of the crushed Brick. It was also used as a measure of temperature while the sample was subject to a constant rate of heating. The samples were bottom loaded in platinum crucibles, and 27.53 mg samples were heated from 30°C to a maximum temperature of 950°C at a constant heating rate of 5°C $min^{-1}$ $min^{-1}$ in an air atmosphere with a purge rate of 75 mL $min^{-1}$.

The solid addition method determined the pH at the point of zero charge $pH_{ZPC}$ [28]. This is done by the addition of a defined quantity of adsorbent 0.1g of crushed Brick to a series of 100 mL Erlenmeyer flasks containing 20 mL of $KNO_3$ solution under shaking for 24 h. Before adding the adsorbent, the pH of each solution was adjusted to be in the range of (1.0–10.0) by the addition of either 0.1 M HCl or 0.1 M NaOH. And pH values were measured at the end of the test ($pH_f$). The $pH_{PZC}$ was determined from the point of intersection of the resulting curve, at which $\Delta pH = 0$.

### 2.4. Batch adsorption experiments

During the study of adsorption of Cr(VI) ions on crushed Brick, batch tests were conducted in room temperature 25±0.2°C. The batch adsorption experiments were conducted by mixing 20 mL of Cr(VI) and 0.4 g of crushed Brick in glass container tubes. Afterwards, these tubes were posed in rotatory shaker on initial concentration of 10 mg $L^{-1}$ at 150 rpm during 80 min at pH 2. Samples for analysis were taken at different time intervals. The suspension was then centrifuged for 5 min at 3000 rpm and the left-out concentration in the supernatant solution was analyzed using UV-Vis spectrophotometer.

The adsorbed amount $q_e$ mg $g^{-1}$ and the percentage removal (R%) of hexavalent chromium uptake by the adsorbent were determined by the following equations

$$q_e = \frac{(C_0 - C_e) \times V}{m} \quad (1)$$

$$R\% = \frac{(C_0 - C_e) \times 100}{C_0} \quad (2)$$

where $C_0$ and $C_e$ mg $L^{-1}$ are the liquid-phase concentration of Cr (VI) at initial time and the equilibrium time, respectively, $V$ (L) is the volume of the solution, and $m$ (g) is the mass of used adsorbent.

## 3. Results and discussion

### 3.1. Chemical composition of crushed Brick:

The chemical composition of crushed Brick is shown in Table 1. This result shows that the presence of silica and alumina are the major constituents along with traces of iron, magnesium, potassium, titanium, sodium and manganese oxides. Heavy metals are present in the natural and the purified clays in trace amounts. The loss on ignition was 11.66% which was analyzed via the method of potassium fluosilicate volumetric and incandesce.

According to the results, the crushed Brick is a typical aluminosilicate mineral with $SiO_2/Al_2O_3$ ratio of 3.65. The chemical composition and the Si/Al ratio of the bricks are very similar to those reported in the literature [29].

### 3.2. FTIR

The FT-IR spectra of crushed Brick before and after adsorption are shown in Fig. 1, The band at 778 $cm^{-1}$ indicates the presence of mineral quartz [30]. The band at 992 $cm^{-1}$ corresponds to Si-O bonds in the $SiO_4$ molecules [31] The absorption at 1618 $cm^{-1}$ was due to the stretching and bending vibration of adsorbed water respectively and the wave number at 3585$cm^{-1}$, assigned to H–O–H stretching vibrations of water molecules weakly hydrogen bonded to the Si–O surface [32]. The third layer-surface hydroxyls formed weak hydrogen bonds and absorb at 3703 $cm^{-1}$ [33]. After the adsorption of Cr(VI), there was no appreciable change observed in the FTIR spectra.

Table 1
Chemical composition of crushed Brick

| Component | Weight % |
|---|---|
| $SiO_2$ | 59.25 |
| $Al_2O_3$ | 16.22 |
| $Fe_2O_3$ | 4.845 |
| MgO | 0.46 |
| MnO | 0.01 |
| ZnO | 0.013 |
| $P_2O_5$ | 0.207 |
| $K_2O$ | 3.55 |
| $Na_2O$ | 2.52 |
| $Cr_2O_3$ | 0.012 |
| $TiO_2$ | 1.16 |
| $SO_3$ | 0.041 |
| L.O.I | 11.66 |

L.O.I : Loss on ignition.

### 3.3. BET and Zeta potential

The results of BET specific surface area, porosity measurements and Zeta potential of crushed Brick are shown in Table 2. Crushed Brick has a surface area of 20.11 $m^{-2}\,g^{-1}$ and it exhibits a net microporosity with a medium pore width of 2.26 Å. On the other hand, the measurement of Zeta potential, which reflects the electrical potential at the interface between crushed Brick particles and the surrounding liquid, shows that the crushed Brick has a negative zeta potential. This indicates that the crushed Brick surface is negatively charged in water at pH7. The present acid-base equilibria are believed to intervene at the water-brick interface when brick is in an equilibrium state with water as shown in Eq. (3) [34].

$$\equiv MOH_{(Brick)} + H_2O \leftrightarrow \equiv MO^-_{(Brick)} + H_30^+ \quad (3)$$

where $M$ represents Al, Fe,etc.

### 3.4. SEM

The result of SEM analysis of crushed Brick is shown in Fig. 2. SEM images, at 100 and 200 µm dimensions show that the crushed Brick has random particle shapes. Furthermore, image at 10 µm shows that the crushed Brick has a

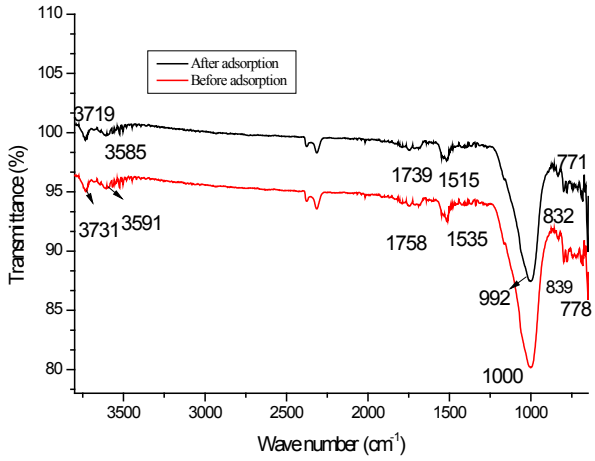


Fig. 1. FTIR spectra of crushed Brick.

Table 2
BET characteristics and zeta potential of the crushed Brick

| | |
|---|---|
| BET surface area ($m^2\,g^{-1}$) | 20.11 |
| Total pore volume ($cm^3\,g^{-1}$) | 0.00944 |
| Average pore diameter (Å) | 2.26 |
| Particle density ($g\,cm^{-3}$) | 3.5678 |
| Zeta potential (mV) | –25.26 |

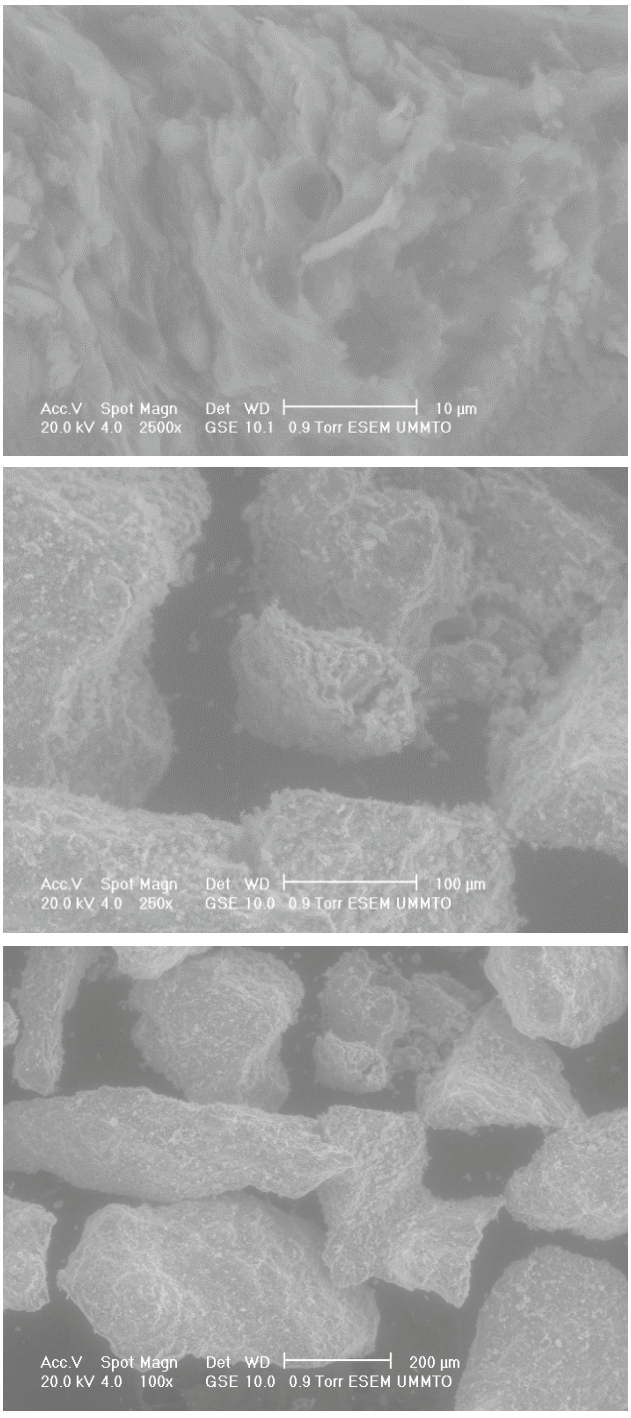


Fig. 2. SEM images of crushed Brick.

matt and porous surface which is good for many types of material.

### 3.5. XRD

The results of crystal structure of crushed Brick obtained by X-ray diffraction (XRD) analysis are shown in Fig. 3. The main crystalline phases obtained in the XRD pattern

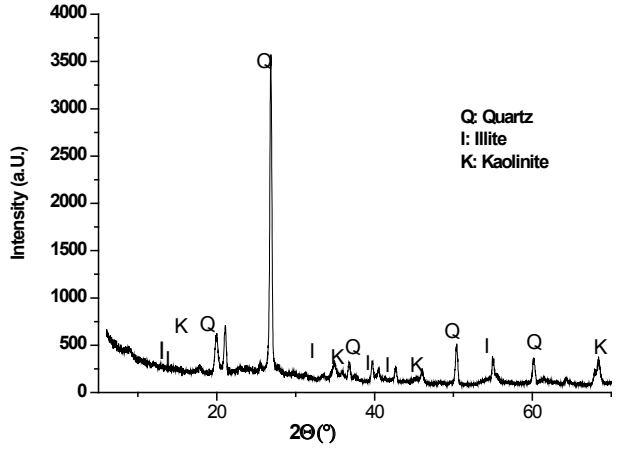


Fig. 3. XRD of crushed Brick.

are quartz (*Q*; 2θ = 26.93°, 21.05°, 26.93°, 39.79°, 50.32° and 60.05°), Illite (*I*; 2θ =17.65°, 35.15°, 40.72°, 42.73°and 54.96°) and kaolinite (*K*; 2θ = 19.97°, 36.85°, 45.98°and 68.28°). XRD pattern also shows the presence of amorphous phase in this material [29].

### 3.6. Thermogravimetric analysis (TGA)

TGA thermo-gravimetric analysis demonstrates the change of material mass with temperature increasing due to the dehydration, decomposition and oxidation of material compounds. The results of TGA analysis of crushed Brick are shown in Fig. 4. Generally, the total thermal weight loss at 800°C was less than 5%. The loss of loosely bound physisorbed water was observed at <215°C [35,36]. The weight loss obtained at 220–420°C indicates the thermal decompositions of the strongly-bonded water molecules present in the first coordination sphere of the interlayer ions [37]. Weight loss above 600°C could be due to the elimination of structural water by releasing OH (dehydroxylation).

### 3.7. Point of zero charge (PZC)

The $pH_{PZC}$ of an adsorbent is a very important characteristic that determines the pH at which the adsorbent surface has net electrical neutrality, and at which value the acidic or basic functional groups no longer contribute to the pH of the solution [38]. Fig. 5 shows a plot of the ΔpH of crushed Brick versus $pH_i$. The $pH_{PZC}$ of the crushed Brick was found to be 4.3, implying that the surface of the crushed Brick is positively charged at pH < 4.3 and negatively charged at pH > 4.3.

## 4. Adsorption testes

### 4.1. Effect of adsorbent mass

The effect of adsorbent mass on the adsorption percentage of Cr(VI) ions onto crushed Brick was studied by changing the quantity of adsorbent (0.06–1.0 g), at volume solution of 20 mL, temperature (25±0.2°C), pH 2 and contact time 80 min and initial concentration of 10 mg $L^{-1}$. Fig. 6

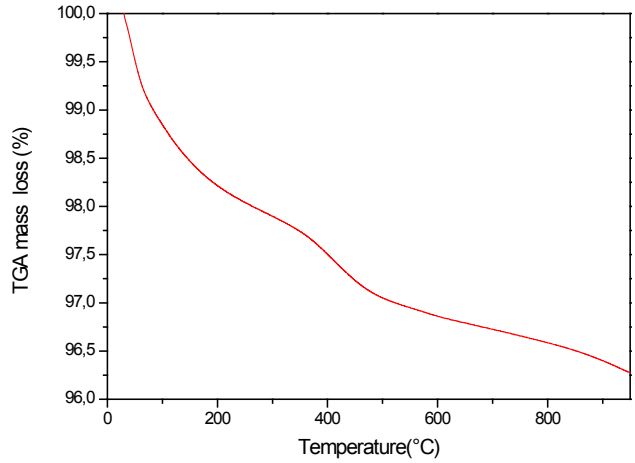


Fig. 4. TGA analysis of crushed Brick.

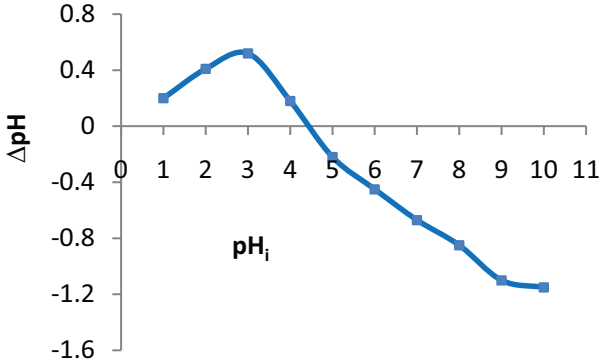


Fig. 5. Point of zero charge of crushed Brick.

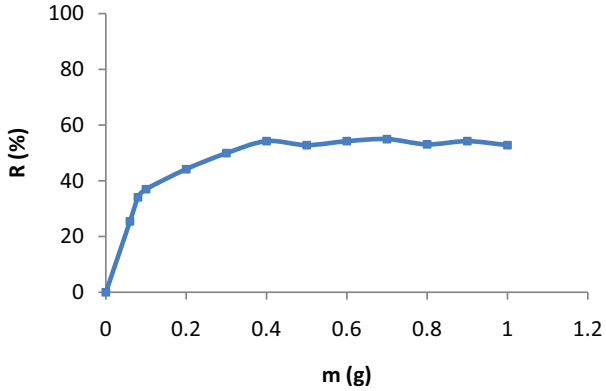


Fig. 6. Effect of adsorbent dose on Cr(VI) removal by crushed Brick, ($m$ = 10 mg L$^{-1}$; agitation speed = 50 rpm; T = 25°C; pH = 2)..

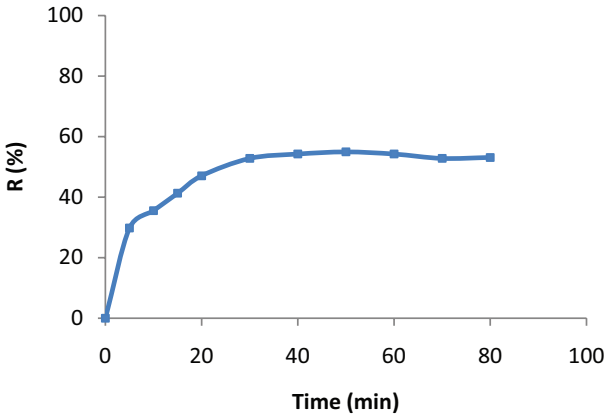


Fig. 7. Effect of contact time on Cr(VI) removal by crushed Brick. ($m$ = 20 g L$^{-1}$; [Cr(VI)]$_0$ = 10 mg L$^{-1}$; agitation speed = 50 rpm; T = 25 °C; pH = 2).

shows that the removal rate of Cr(VI) increases from 25.46% to 54.24% and thereafter it remained approximately constant at 0.4 g. This behavior can be attributed to the availability of more adsorption sites and greater surface area with adsorbent mass increasing [39,40]. 20 g L$^{-1}$ value was chosen for the study of the subsequent parameters.

### 4.2. Effect of contact time

Contact time is an important parameter because it determines the adsorption kinetics of an adsorbent at a given initial concentration of the adsorbate [41].

The adsorption processes were almost accomplished in the first 5 min and reached equilibrium within 30 min as shown in Fig. 7. It was observed from the beginning that the adsorption was fast in the initial stage as a result of the large number of available and reached equilibrium within 30 min. After a certain period of time, the reaction slows down as the process is attenuated, as the number of vacant sites decreases [42].

### 4.2. Effect of agitation speed

The effect of stirring speed on the removal rate was investigated at different stirring speeds such as 50, 100 and 150 rpm at initial Cr(VI) concentration of 10 mg L$^{-1}$ and room temperature. According to Fig. 8 data shows that the achievement of a constant value of adsorption capacities of Cr(VI) practically independent on the stirring speed employed at the range of 50–150 rpm, and no difference of adsorption quantity was insignificant as the stirring speed increases. Similar phenomena were observed in the kinetic experiments of MB on activated carbon and on Perlite [43,44].

### 4.4. Effect of initial Cr(VI) concentration

The effect of initial concentration of Cr(VI) in range of 5 mg L$^{-1}$ to 90 mg L$^{-1}$ on the removal efficiency using crushed Brick is shown in Fig. 9. The experiments were carried out using fixed adsorbent dose of 20 g L$^{-1}$ at ambient temperature (25 ± 0.2°C), pH 3 and 50 rpm. It was observed that the percentage of Cr(VI) removal decreases with increasing in initial Cr(VI) concentration (73.71% to 51.43%). This is may be due to the less availability of the active sites of the adsorbent which could be saturated at higher Cr(VI) concentrations [45]. In addition, the adsorbed negatively charged Cr(VI) ion electrostatically repels the incoming sor-

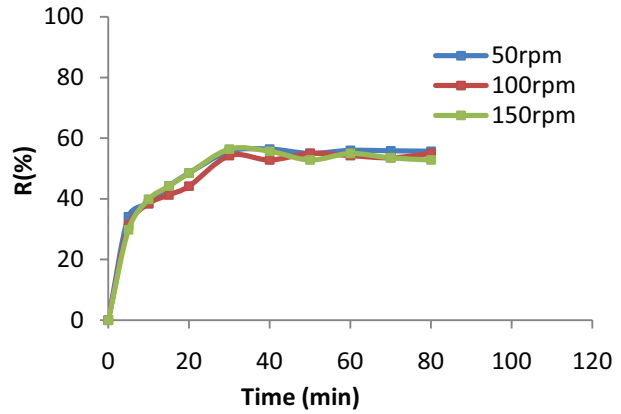


Fig. 8. Effect of agitation speed on Cr(VI) removal by crushed Brick ($m$ = 20 g $L^{-1}$; $[Cr(VI)]_0$ = 10 mg $L^{-1}$; T = 25°C; pH = 2).

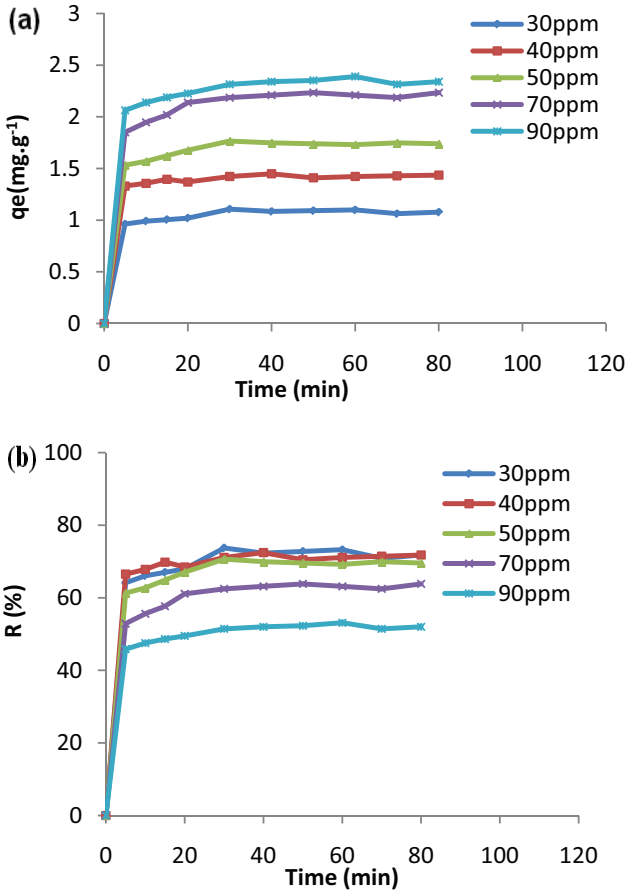


Fig. 9. Effect of initial Cr(VI) concentration on the adsorption capacity (a) and removal (b) of crushed Brick (m = 20 g $L^{-1}$; agitation speed = 50 rpm; T = 25 °C; pH = 3).

bet ions resulting in decrease of the adsorption percentage [46]. However, the adsorption capacity increased form 1.10 mg $L^{-1}$ to 2.31 mg $L^{-1}$ as Cr(VI) concentration raises. This is due to higher probability of collision between Cr(VI) ions and crushed Brick which resulted in the increased driving force of the concentration gradient [47,48].

### 4.5. Effect of pH

The pH of the solution has an important role in the adsorption process. The effect of pH on Cr(VI) adsorption was examined at pH values from 1 to 7 and was evaluated separately in a set of batch experiments as shown in Fig. 11 . It is well known that Cr(VI) can exist in solution in the following ionic forms: chromate ($CrO_4^{-2}$), dichromate ($Cr_2O_7^{-2}$) or hydrogen dichromate ($HCrO_4^-$), which is governed by solution pH and total chromium concentration [49]. Thus, the amount of adsorbed Cr(VI) is higher in acidic environment. However, when pH is lesser than 2, the Cr(VI) in water is in the form of $H_2CrO_4$ [50], therefore, the Cr(VI) adsorption on crushed Brick decreases as shown in Fig. 11. While the highest adsorption of Cr(VI) was found at pH 3 where the combined effect of increase in electrostatic force of attraction between positive charge surface of the crushed Brick and $HCrO_4^-$ and faster intra-particle diffusion may account for maximum adsorption efficiency [51,52]. As a result, the mechanism of Cr(VI) adsorption onto crushed Brick at acidic pH could be regarded as in the following process Fig. 10:

Where M represents Al, Fe, etc.

Based on the experiment of the $pH_{ZPC}$ of the crushed Brick which was about 4.3 in its value as shown in Fig. 6 and the negatively zeta potential value in Table 2 are related to the stability of crushed Brick dispersions indicating the degree of repulsion between adjacent, similarly charged particles in the dispersion. During the adsorption, the concentrations of surface species ≡MOH uncharged surface groups, $\equiv MOH_2^+$ positive charged surface groups, $\equiv MO^-$ negatively charged groups) change at different pH values. With increasing pH higher than 4.3, the number of negatively charged $\equiv MO^-$ groups increases and this leads to the decrease of hexavalent chromium adsorption due to the electrostatic repulsion [53]. The surface charge of crushed Brick was positive at pH below the $pH_{ZPC}$ Consequently, Cr(VI) would be adsorbed across the electrostatic attraction and/or via the combination of $HCrO_4^-$ to acidic functional groups on the surface of crushed Brick [54]. Similar results have been obtained previously [55–58].

### 4.6. Effect of temperature

Batch experiments were performed at temperatures such as 25°C, 35°C and 45°C. As shown in Fig. 12, with an increase in solution temperature, Cr(VI) removal percentage decreased from 55% at 25°C to 44% at 35°C and 35% at 45°C. It may be due to a decrease in the degree of freedom of adsorbed species and a decrease in available adsorption active sites which indicates that the adsorption phenomenon is exothermic [59]. This is the typical case of microporous solids.

## 5. Adsorption isotherm studies

An adsorption isotherm describes the relationship between the amount of adsorbate adsorbed on the adsorbent and the concentration of dissolved adsorbate in the liquid at equilibrium. As shown in Fig. 13, the shape of the curves $q_e$ vs. $C_e$ clearly indicated that the isotherm belongs to L type according to the classification of equilibrium isotherm in solution by Giles et al. [60].

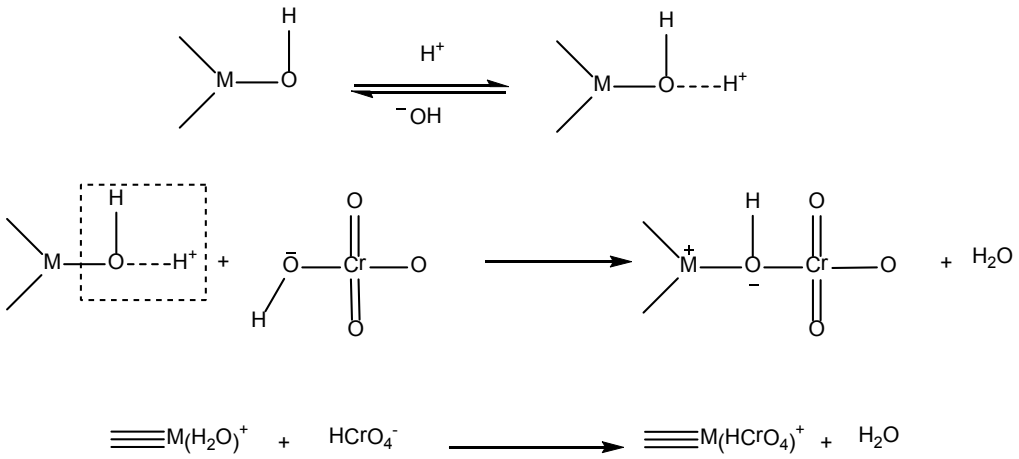


Fig. 10. The mechanism of adsorption of Cr(VI) onto crushed Brick at acidic medium.

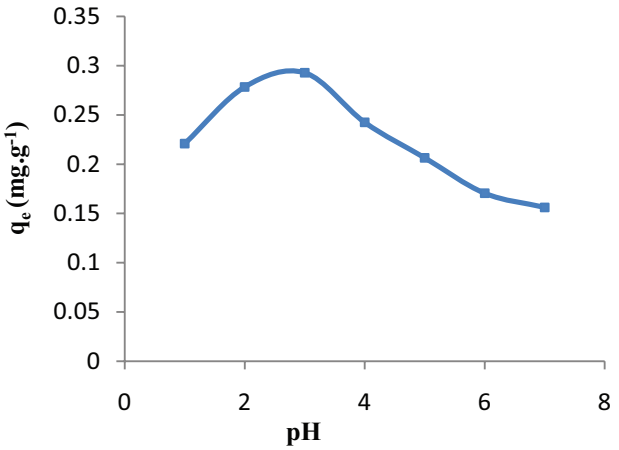


Fig. 11. Effect of pH on the adsorption capacity of crushed Brick for the removal of Cr(VI). (m = 20 g $L^{-1}$; agitation speed = 50 rpm; [Cr(VI)] = 10 mg $L^{-1}$; T = 25°C).

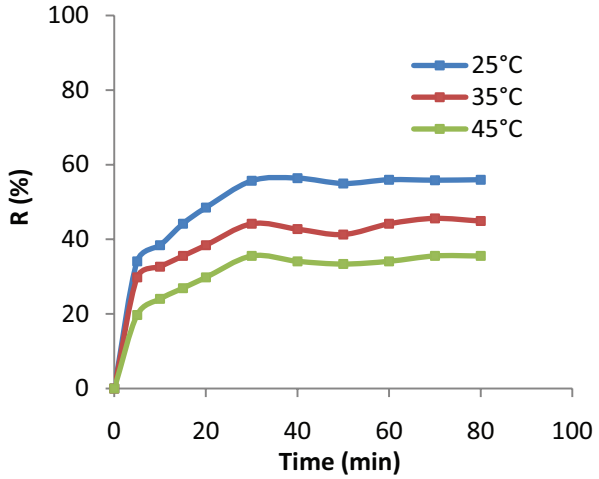


Fig. 12. Effect of temperature on Cr(VI) removal by crushed Brick. (m = 20 g $L^{-1}$; agitation speed = 50 rpm; $[Cr(VI)]_0$ = 10 mg $L^{-1}$; T = 25°C; pH = 3).

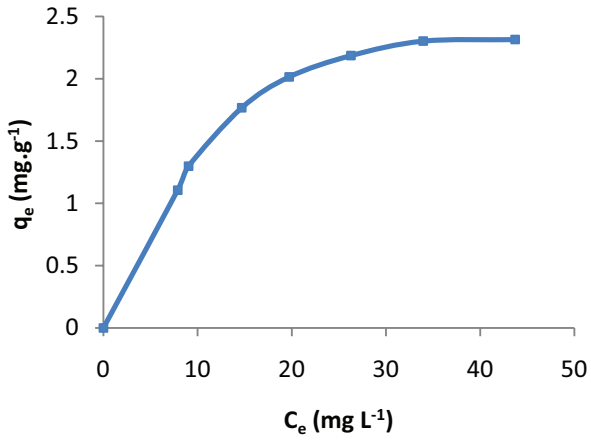


Fig. 13. Equilibrium isotherm of Cr(VI) adsorption onto crushed Brick.

### 5.1. Langmuir isotherm

The Langmuir model assumes that the uptake of metal ions occurs on a homogeneous surface by monolayer adsorption without any interaction between adsorbed ions [61]. The Langmuir equation in the linear form is expressed as Eq. (4):

$$\frac{C_e}{q_e} = \frac{1}{q_m \cdot K_L} + \frac{C_e}{q_m} \tag{4}$$

With $q_m$ mg $g^{-1}$: maximum amount of chromium adsorbed, $q_e$ mg $g^{-1}$: equilibrium amount of adsorbent, $K_L$ L $mg^{-1}$: Langmuir constant and $C_e$ mg $L^{-1}$: residual concentration of solute at equilibrium. The Langmuir constants related to adsorption capacity and energy, respectively. The plot of $C_e/q_e$ against $C_e$ in Fig. 14(a).

The essential characteristics of the Langmuir isotherm can be expressed by a dimensionless constant called the separation factor $R_L$ [62]:

$$R_L = \frac{1}{1 + K_L C_0} \tag{5}$$

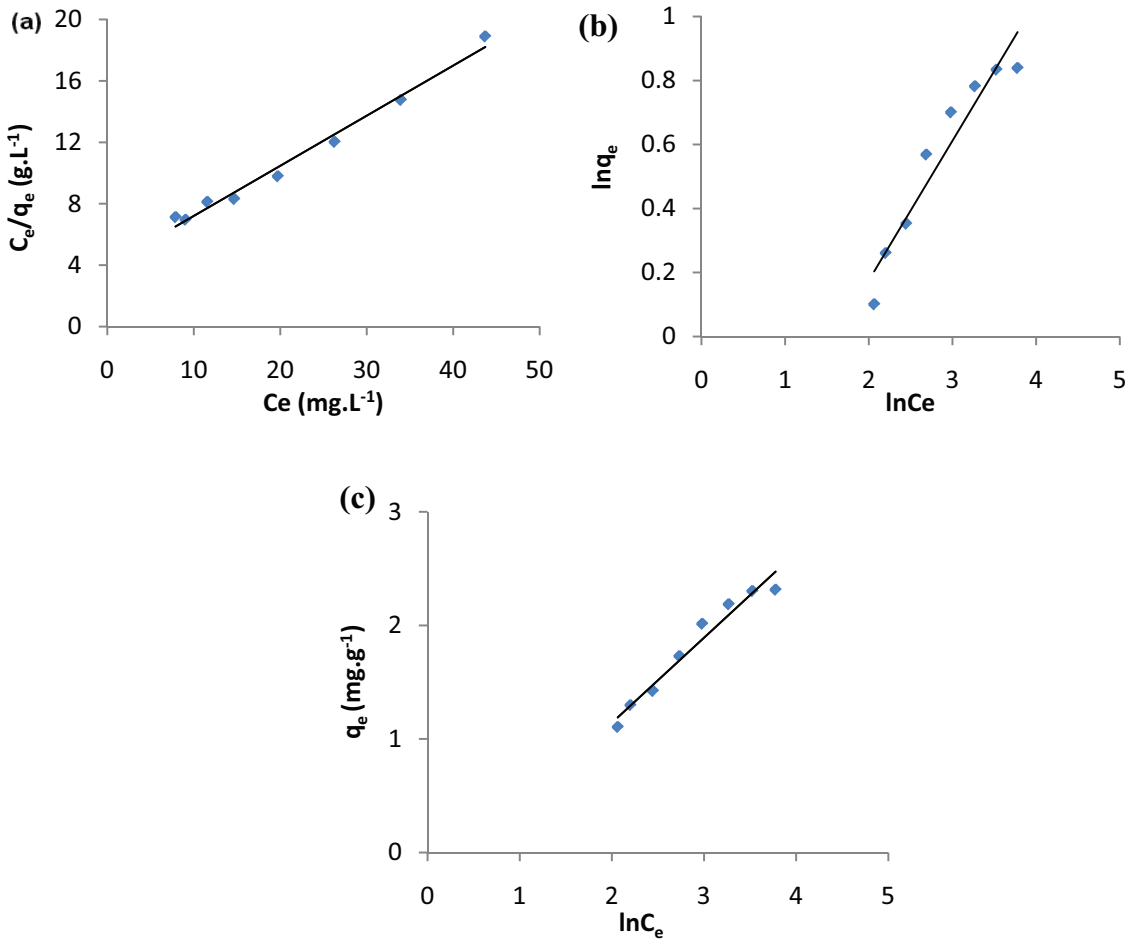


Fig. 14. Modeling of Cr(VI) adsorption onto crushed Brick using parameter isotherms: Langmuir, (b) Freundlich, (c) Temkin.

where $C_0$ is the initial concentration of metal ion (mg $L^{-1}$). The value of $R_L$ indicated the type Langmuir isotherm. $R_L$ value demonstrates a variable nature of adsorption to be either unfavorable if $R_L$ >1, linear if $R_L$ =1, favorable if 0 < $R_L$ < 1 and irreversible if $R_L$ =0. From the data calculated in Table 3, the $R_L$ is greater than 0 but less than 1 indicating that Langmuir isotherm is favorable.

Table 3
Langmuir isotherm constant

| $C_0$ | $R_L$ |
|---|---|
| 5 | 0.719 |
| 10 | 0.562 |
| 15 | 0.461 |
| 20 | 0.391 |
| 40 | 0.243 |
| 60 | 0.176 |
| 90 | 0.125 |

### 5.2. Freundlich isotherm

Freundlich's equation is an empirical model based on heterogeneous adsorption over independent sites. The equation is written in linear form as follows [63]:

$$\ln q_e = \ln K_F + \frac{1}{n}\ln C_e \quad (6)$$

$K_F$ and $n$ are the Freundlich constants. Here, $n$ giving a sign of how congruent the adsorption process is, and $K_F$ $mg^{1-1/n}$ $L^{1/n}g^{-1}$ represents the quantity of chromium adsorbed on the adsorbent for a unit equilibrium concentration. The values of $K_F$ and $n$ were determined from the intercept and slope of the linear plot of ln $q_e$ versus ln $C_e$ in Fig. 14(b), respectively, and the results are presented in Table 4. The $n$ value indicates the degree of nonlinearity between solution concentration and adsorption as follows: if $n$ = 1, then adsorption is linear; if $n$ < 1, then adsorption interpreted as a chemical process; if $n$ > 1, then adsorption can be referred to as a physical process. $n$ value in Freundlich within the range of 1–10 represents good adsorption [64].

### 5.3. Temkin isotherm

Adsorbent–adsorbate interactions form a crucial factor for this isotherm. By lifting out the ultimate low and high

Table 4
Isotherm parameters for Cr(VI) onto crushed Brick obtained by using the linear method

| Isotherm | Isotherm constants | |
|---|---|---|
| Langmuir | $q_{e,cal}$ (mg g$^{-1}$) | 3.067 |
| | $q_{e,(exp)}$ (mg g$^{-1}$) | 2.310 |
| | $K_L$ (L mg$^{-1}$) | 0.082 |
| | $R^2$ | 0.985 |
| Freundlich | $K_F$ (mg$^{1-1/n}$ L$^{1/n}$ g$^{-1}$) | 0.497 |
| | $n$ | 2.290 |
| | $R^2$ | 0.921 |
| Temkin | $A_T$ (L g$^{-1}$) | 0.619 |
| | $B$ | 0.749 |
| | $R^2$ | 0.959 |

concentration values, the model assumes that the heat adsorption (function of temperature) of all molecules in the layer would decrease linearly rather than logarithmically in coverage [65]. In Fig. 14c, the Temkin isotherm has been generally applied in the following equations [66,67]:

$$q_e = \left(\frac{RT}{b_T}\right)\ln(A_T C_e) \tag{7}$$

$$q_e = \frac{RT}{b_T}\ln A_T + \left(\frac{RT}{b_T}\right)\ln C_e \tag{8}$$

where $B_T = \frac{RT}{b_T}$

$A_T$ is the equilibrium binding constant Lg$^{-1}$, $b_T$ is the adsorption constant J mol$^{-1}$, $R$ is a universal gas constant 8.314 J mol$^{-1}$ K$^{-1}$, T is absolute temperature value [298 K]. The constants parameters of Temkin isotherm were determined from the linear curve of ($q_e$) vs. ln($C_e$).

In Table 4, the maximum monolayer coverage capacity ($q_m$) from Langmuir isotherm model is determined to be 3.06 mg g$^{-1}$, $K_L$ (Langmuir isotherm constant) is 0.078 (L mg$^{-1}$). The $R_L$ values for the adsorption of Cr(VI) onto crushed Brick are in the range of (0.719 – 0.125) (see Table 3). When $R_L$ is less than the unity values, it indicates that the equilibrium sorption is favorable, and the high determination coefficient $R^2$ value is 0.984 proving that the sorption data fits well to Langmuir Isotherm model then the Temkin and Freundlich models. Hence, it can be understood that, the Langmuir and Temkin isotherms are the most suitable models for the sorbate-sorbent system.

## 6. Adsorption kinetic experiments

### 6.1. Pseudo-first-order and second-order kinetic models

The pseudo first order and pseudo-second-order reaction models were applied to study the kinetics of the adsorption process. The experimental data were fitting for these two orders. The linear forms of kinetic equations are given as [68,69]:

$$\ln(q_e - q_t) = \ln q_e - k_1 t \tag{9}$$

$$\frac{t}{q_t} = \frac{1}{k_2 q_e^2} + \frac{1}{q_e} t \tag{10}$$

where $q_e$ is the amount of adsorbate adsorbed at equilibrium (mg g$^{-1}$), $q_t$ is the amount of adsorbate adsorbed at time t (min), $k_1$ and $k_2$ are the constant rates of pseudo-first-order and pseudo-second-order respectively. Kinetic plots of ln($q_e$ – $q_t$) vs. $t$ for pseudo-first-order and a plot of $t/q_t$ vs. $t$ for pseudo-second-orders are given in (Figs. 15a and b).

As shown in Table 5, the comparison made between the experimental adsorption capacity ($q_e$. exp) values and the calculated adsorption capacity values capacity ($q_e$. cal), showed that the calculated capacity ($q_e$. cal) values were similar to the experimental capacity ($q_e$. exp) values for the pseudo-first-order kinetics. On the other hand, the calculated value capacity ($q_e$. cal) estimated from the pseudo-second-order kinetic model gave very close values compared to experimental value. In addition, the correlation coefficient values for pseudo-second-order model were higher than that of pseudo-first-order model. Based on $R^2$ values, it was confirmed that pseudo-second-order model best fits the adsorption data. These results are consistent with other studies [70,71].

### 6.2. Intra-particle diffusion model

In Fig. 15(c), the adsorption process may not only be a diffusion (external mass transfer) but it may also be controlled by the intra-particle diffusion [72]. The equations used to confirm the diffusion mechanism can be defined by Eq. (11):

$$q_t = q_{dif} t^{0.5} + C \tag{11}$$

where $q_{diff}$ (mg g$^{-1}$ min$^{-0.5}$) is the intra-particle diffusion rate constant. The Boyd model provides information as to whether the rate controlling step results from film diffusion (boundary layer) or particle diffusion (diffusion inside the pores) [73].

During the adsorption process, three linear regions appeared on the curve as a result of three possible steps as in [74,75]: an external mass transfer step such as the boundary layer diffusion occurred first, then an intra-particle diffusion step for the second and lastly a saturation step. In this study, the first linear region with a high slope signaled a rapid external diffusion stage depicting macro-pore or inter-particle diffusion which is different from the second step, gradual adsorption stage controlled by intra-particle (micropore) diffusion, and the last step (saturation stage). This observation can also be linked to adsorption mechanisms mainly involving the surface layers of crystallites [76].

## 7. Thermodynamic study

The temperature effect on the adsorption of hexavalent chromium was studied in order to obtain the relevant thermodynamic parameters. The free energy of

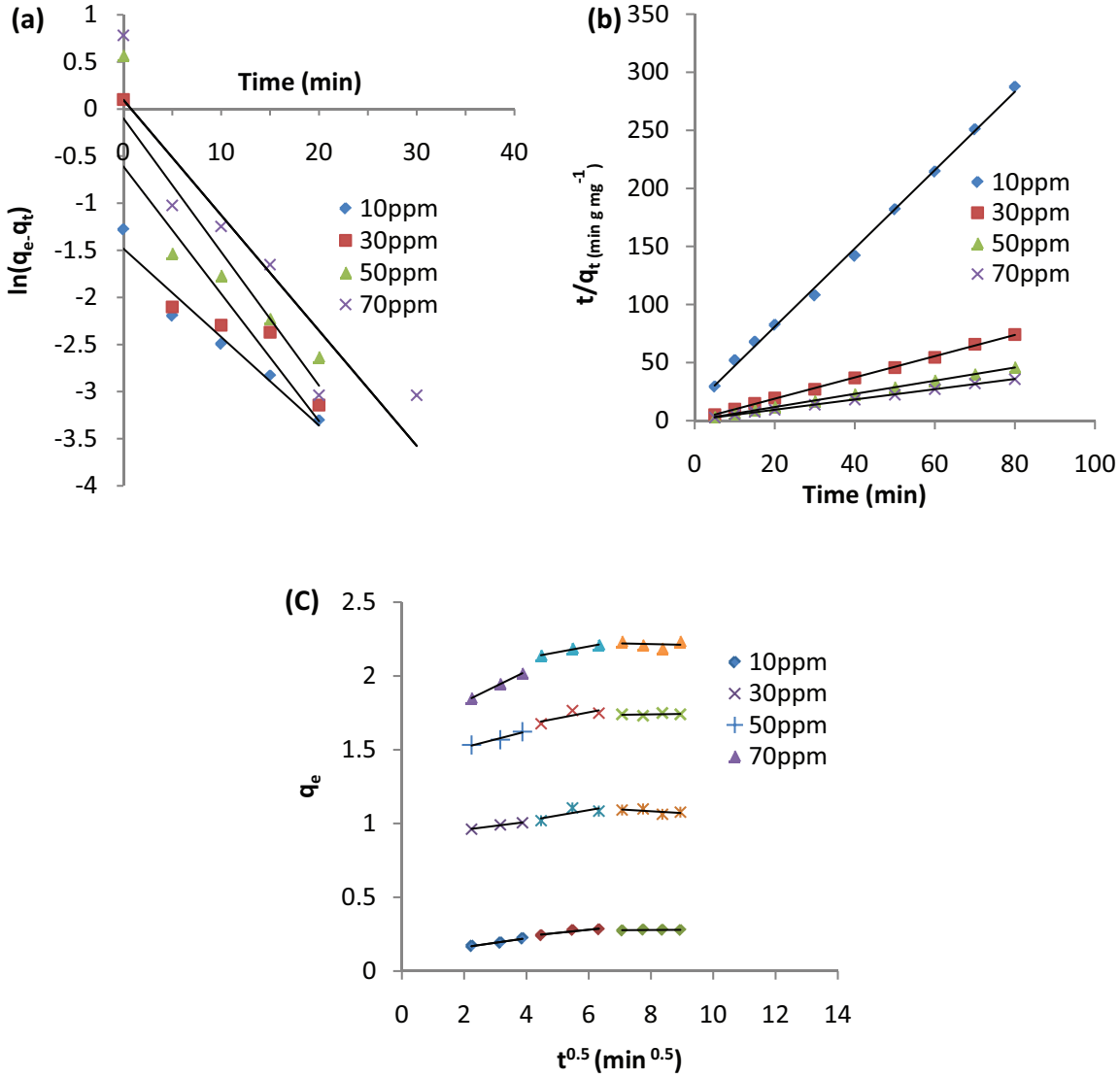


Fig. 15. Plot of (a) the pseudo-first-order, (b) the pseudo-second-order, (c) the intra-particle diffusion model.

Table 5
Parameters of kinetic models for Cr(VI) adsorption on the crushed Brick

| Model | Parameters | Initial concentration of Cr(VI) | | | |
|---|---|---|---|---|---|
| | | 10 | 30 | 50 | 70 |
| | $q_{e,exp}$ (mg g$^{-1}$) | 0.278 | 1.105 | 1.766 | 2.185 |
| Pseudo-first-order | $q_{e,cal}$ (mg g$^{-1}$) | 0.227 | 0.543 | 0.905 | 1.107 |
| | $k_1$ (min$^{-1}$) | 0.093 | 0.135 | 0.141 | 0.122 |
| | $R^2$ | 0.951 | 0.767 | 0.817 | 0.852 |
| Pseudo-second -order | $q_{e,cal}$ (mg g$^{-1}$) | 0.296 | 1.092 | 1.766 | 2.262 |
| | $k_2$ (g mg$^{-1}$ min$^{-1}$) | 0.846 | 1.278 | 0.652 | 0.347 |
| | $R^2$ | 0.997 | 0.999 | 0.999 | 0.999 |
| Intra-particle diffusion | $k_{diff}$ | 0.030 | 0.026 | 0.054 | 0.102 |
| | $C$ (g mg$^{-1}$ min$^{-0.5}$) | 0.100 | 0.903 | 1.407 | 1.621 |
| | $R^2$ | 0.975 | 0.987 | 0.964 | 1.000 |

adsorption (ΔG°), the entropy (ΔS°) and enthalpy change (ΔH°) in the adsorption process are related to the Van't Hoff equations [77]:

$$\Delta G^\circ = -RT\ln K_c \tag{12}$$

$$\ln K_C = \frac{\Delta S^0}{R} - \frac{\Delta H^0}{R\,T} \tag{13}$$

$$K_c = \frac{C_{Ae}}{C_{Se}}$$

where $\ln K_c$ [78] is the constant of equilibrium, $C_{Ae}$ is the amount of adsorbate on the adsorbent per volume of the solution (L) at equilibrium (mg $L^{-1}$), $C_{Se}$ is the equilibrium concentration of adsorbate in the aqueous solution (mg $L^{-1}$), R is the gas constant 8.314 J $K^{-1}$ $mol^{-1}$ and T is the temperature (*K*). Therefore, the values of (ΔH°) and (ΔS°) were obtained from the slope and intercept of the $\ln K_c$ versus 1/T curve according to Fig. 16. The negative value of (ΔS°) indicates the favorable nature of the adsorption phenomenon. Moreover, the negative values of enthalpy change revealed that the adsorption process was exothermic. The positive value of (ΔG°) confirmed that the sorption is non-spontaneous in nature. The magnitude of (ΔH°) may be used to distinguish between chemisorption bond strengths that are generally in the range of (+84) – (+420)( kJ $mol^{-1}$) while physisorption bond strengths are <+84 kJ $mol^{-1}$ [79]. From Table 6, the weak (ΔH°) value is –32.47 kJ $mol^{-1}$ and therefore confirms that Cr(VI) adsorption by crushed Brick occurs more according to a physisorption process rather than a pure chemical adsorption mechanism [34]. The Gibbs energy (ΔG°) increased when the temperature was increased from 25 to 45°C indicating a decrease in feasibility of adsorption at higher temperature. It is important to note that (ΔG°) value up to 4.78 4.78 kcal $mol^{-1}$ (20 kJ $mol^{-1}$) is consistent with electrostatic interaction between adsorption sites and ionic species (physical adsorption) [80].

Table 7 shows a brief summary of adsorption capacities of some adsorbents for Cr(VI) removal compared with crushed Brick used in this study. It is noteworthy that the crushed Brick powder has an acceptable adsorption capacity for Cr(VI) removal compared to other adsorbents. Due to the large availability of brick waste, this material could be used as an alternative adsorbent for water treatment.

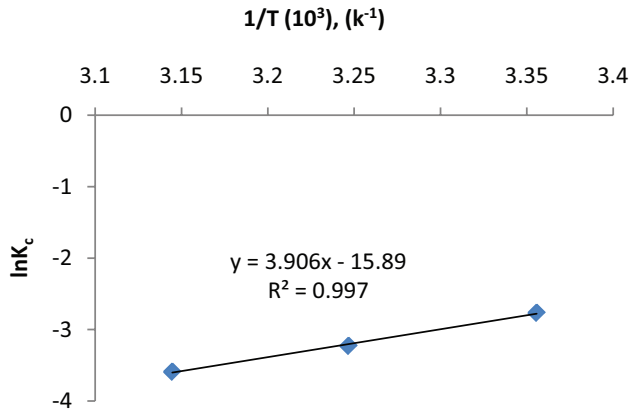


Fig. 16. Plot of Van't Hoff equation.

Table 6
Thermodynamic parameters of the Cr(VI) adsorption on crushed Brick

| Temperature | ΔH° (kj $mol^{-1}$) | ΔS° (kj $mol^{-1}$ $K^{-1}$) | ΔG° (kj $mol^{-1}$) |
|---|---|---|---|
| 25°C | –32.47 | –132.11 | 6.89 |
| 35°C | | | 8.22 |
| 45°C | | | 9.54 |

## 8. Determination of the adsorption activation energy

The adsorption activation energy $E_a$ was obtained by the use of the Arrhenius equation Eq. (14) where it is possible to gain some insight into the type of adsorption.

$$\ln k_2 = \ln A - \frac{E_a}{RT} \tag{14}$$

In Fig. 17, $E_a$ is the activation energy (J $mol^{-1}$), $k_2$ the pseudo-second-order rate constant for adsorption (g $mg^{-1}$

Table 7
Adsorption of Cr(VI) by various adsorbents

| Adsorbent | $q_m$ (mg $g^{-1}$) | Reference |
|---|---|---|
| Fireclay | 0.23 | [81] |
| Soya cake | 0.28 | [82] |
| Kaolin | 0.571 | [83] |
| Spent activated clay | 0.743-1.422 | [80] |
| Modified oak sawdust | 1.70 | [84] |
| Activated carbon | 2.84 | [85] |
| Crushed Brick | 3.06 | This work |
| Na-montmorillonite (dynamic mode) | 5.13 | [86] |
| ZeoliteNaX | 6.414 | [87] |

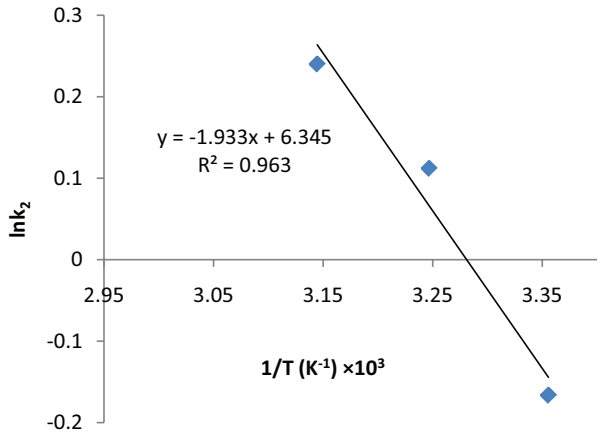


Fig. 17. Plot of the Arrhenius equation.

$min^{-1}$), $A$ the temperature-independent Arrhenius factor (g $mol^{-1}$ $S^{-1}$), $R$ the gas constant 8.314 (J $K^{-1}mol^{-1}$) and T the solution temperature (K) The slope of the plot of $\ln k_2$ vs. $T^{-1}$ can then be used to evaluate $E_a$.

Low activation energies 5–40 (kJ $mol^{-1}$) are characteristic of physical adsorption while higher ones 40–800 (kJ $mol^{-1}$) suggest chemisorption [88]. The present results give $E_a$ = +16.08 (kJ $mol^{-1}$) for the adsorption of Cr(VI) onto crushed Brick indicating that the adsorption has a low potential barrier and corresponds therefore to physisorption.

## 9. Conclusions

The construction waste "crushed Brick" was successfully used as an adsorbent for the removal of Cr(VI) from water. Different operating parameters were studied. The used crushed Brick has a surface area of 20.11 $m^2 g^{-1}$ and it exhibits a net microporosity with a medium pore width of 2.26 Å. The adsorption experiments showed that Cr(VI) adsorption is more favorable at acidic medium. Moreover, it decreases with an increasing temperature. Hence, the maximum adsorption capacity of crushed Brick was 3.06 mg $g^{-1}$. The results also show that the pseudo-second-order reaction kinetics and the intra- particle diffusion model provide the best description of the adsorption. The experimental data for the adsorption process demonstrates that the Langmuir adsorption isotherm model is better than the Temkin and Freundlich adsorption models. Thermodynamic parameters have been also evaluated for the system and have provided that the adsorption is exothermic in nature, non-spontaneous and mainly physical. Overall, the uses of such as a kind of materials are a double-win for both water treatment and valorization of wastes.

## Symbols

$A_T$ — Temkin isotherm equilibrium binding constant, (L $g^{-1}$)
$A$ — Temperature-independent Arrhenius factor (g $mol^{-1}$ $s^{-1}$)
$b_T$ — Temkin isotherm constant, (J $mol^{-1}$)
$C_0$ — Initial Cr(VI) concentration (mg $L^{-1}$)
$C_{Ae}$ — Amount of adsorbate on the adsorbent per volume of the solution at equilibrium, (mg $L^{-1}$)
$C_d$ — Equilibrium concentration of adsorbate in the aqueous solution, (mg $L^{-1}$)
$C_e$ — Cr(VI) concentration in solution at equilibrium, (mg $L^{-1}$)
$C_{Se}$ — Equilibrium concentration of adsorbate in the aqueous solution, (mg $L^{-1}$)
$E_a$ — Activation energy (J $mol^{-1}$)
$\Delta G°$ — Standard free energy, (kJ $mol^{-1}$)
$\Delta H°$ — Standard enthalpy change, (kJ $mol^{-1}$)
$K_1$ — Pseudo-first-order rate constant, ($min^{-1}$)
$K_2$ — Pseudo-second-order rate constant, (g $mg^{-1}$ $min^{-1}$)
$K_c$ — Equilibrium constant
$K_F$ — Freundlich isotherm constant, ($mg^{1-1/n}L^{1/n}$ $g^{-1}$)
$K_L$ — Langmuir constant, (L $mg^{-1}$)
$m$ — Amount of biosorbent, (g)
$n$ — Freundlich exponent
$q_{e(exp)}$ — Experimental adsorption capacity, (mg $g^{-1}$)
$q_{e(cal)}$ — Calculated adsorption capacity, (mg $g^{-1}$)
$q_t$ — Amount of adsorbate adsorbed at time t, (mg $g^{-1}$)
$q_m$ — Maximum monolayer coverage capacity, (mg $g^{-1}$)
$q_{dif}$ — Intraparticle diffusion rate constant, (mg $g^{-1}$ $min^{-0.5}$)
$R$ — Gas constant (8.314 J $K^{-1}$ $mol^{-1}$)
$R$ (%) — Percentage of removal, (%)
$R_L$ — Separation factor
$\Delta S°$ — Entropy (kJ $mol^{-1}K^{-1}$)
$T$ — Absolute temperature, (K)
$t^{0.5}$ — $min^{-0.5}$
$V$ — Volume of the solution, (L)
$pH_{PZC}$ — The pH of point of zero charge
$pH_i$ — The initial pH of the solution
$pH_f$ — The final pH of the solution
$\Delta pH$ — The diference between $pH_f$ and $pH_i$

## Acknowledgments

The authors gratefully acknowledge financial support from the Algerian Ministry of Higher Education and Scientific Research.

## References

[1] V.K. Gupta, M. Gupta, S. Sharma, Process development for the removal of lead and chromium from aqueous solutions using red mud, an aluminium industry waste, Wat. Res., 35 (2001) 1125–1134.
[2] C. Namasivayam, R.T. Yamuna, Adsorption of chromium (VI) by a low-cost adsorbent: Biogas residual slurry, Chemosphere, 30 (1995) 561–578.
[3] M.H. Dehghani, M.M. Taher, A.K. Bajpai, B. Heibati, I. Tyagi, M. Asif, S. Agarwal, V.K. Gupta, Removal of noxious Cr (VI) ions using single-walled carbon nanotubes and multi-walled carbon nanotubes, Chem. Eng. J., 279 (2015) 344–352.
[4] S.C.W. Sakti, Y. Narita, T. Sasaki, Nuryono, S. Tanaka, A novel pyridinium functionalized magnetic chitosan with pH-independent and rapid adsorption kinetics for magnetic separation of Cr(VI), J. Environ. Chem. Eng., 3 (2015) 1953–1961.
[5] P.K. Tyagi, Study of potentiality of coal fly ash for the removal of Cr(VI) from industrial wastewater: equilibrium and kinetic studies, Int. J. Eng. Technol. Sci. Res., 4 (2017) 836–843.
[6] G.B. Post, A.H. Stern, Comments on article "Toxicity and carcinogenicity of chromium compounds in humans" by Costa and Klein, Crit. Rev. Toxicol., 36 (2006) 777–778.
[7] R. Djellabi, F.M. Ghorab, S. Nouacer, A. Smara, O. Khireddine, Cr(VI) photocatalytic reduction under sunlight followed by Cr(III) extraction from $TiO_2$ surface, Mater. Lett., 176 (2016) 106–109.
[8] K. Industry, W. Water, Efficiency of removing chromium from plating industry wastewater using the electrocoagulation method, Q. Int. Arch. Heal. Sci., 2 (2015) 83–87.
[9] P.A. Vinodhini, P.N. Sudha, Removal of heavy metal chromium from tannery effluent using ultrafiltration membrane, Text. Cloth. Sustain., 2 (2017) 5.
[10] M.M. Matlock, B.S. Howerton, D.A. Atwood, Chemical precipitation of heavy metals from acid mine drainage, Water Res., 36 (2002) 4757–4764.
[11] X. Li, P.G. Green, C. Seidel, C. Gorman, J.L. Darby, Chromium removal from strong base anion exchange waste brines, J. Am. Water Works Assoc., 108 (2016) E247–E255. doi:10.5942/jawwa.2016.108.0049.

[12] W. Jiang, M. Pelaez, D.D. Dionysiou, M.H. Entezari, D. Tsoutsou, K. O'Shea, Chromium(VI) removal by maghemite nanoparticles, Chem. Eng. J., 222 (2013) 527–533. doi:10.1016/j.cej.2013.02.049.
[13] S. Rangabhashiyam, N. Selvaraju, B. Raj Mohan, P.K. Muhammed Anzil, K.D. Amith, E.R. Ushakumary, Hydrous cerium oxide nanoparticles impregnated enteromorpha sp. for the removal of hexavalent chromium from aqueous solutions, J. Environ. Eng. (United States), 142 (2016) 1–9.
[14] T.S. R. Djellabi, M.F. Ghorab, Simultaneous removal of methylene blue and hexavalent chromium from water using $TiO_2$/Fe(III)/sunlight, CLEAN – Soil, Air, Water, 45 (2017) 1500379.
[15] I. Professor, M. Moradi, A. Dehpahlavan, R. Rezaei Kalantary, A. Ameri, M. Farzadkia, H. Izanloo, Application of modified bentonite using sulfuric acid for the removal of hexavalent chromium from aqueous solutions, Environ. Heal. Eng. Manag. J., 2 (2015) 99–106.
[16] S. Rangabhashiyam, N. Selvaraju, Adsorptive remediation of hexavalent chromium from synthetic wastewater by a natural and $ZnCl_2$ activated Sterculia guttata shell, J. Mol. Liq., 207 (2015) 39–49.
[17] S. Rangabhashiyam, E. Nakkeeran, N. Anu, N. Selvaraju, Biosorption potential of a novel powder, prepared from Ficus auriculata leaves, for sequestration of hexavalent chromium from aqueous solutions, Res. Chem. Intermed., 41 (2015) 8405–8424.
[18] S. Rangabhashiyam, E. Suganya, A.V. Lity, N. Selvaraju, Equilibrium and kinetics studies of hexavalent chromium biosorption on a novel green macroalgae Enteromorpha sp., Res. Chem. Intermed., 42 (2016) 1275–1294.
[19] S. Rangabhashiyam, N. Selvaraju, Evaluation of the biosorption potential of a novel Caryota urens inflorescence waste biomass for the removal of hexavalent chromium from aqueous solutions, J. Taiwan Inst. Chem. Eng., 47 (2015) 59–70.
[20] N. Saranya, E. Nakeeran, M.S. Giri Nandagopal, N. Selvaraju, Optimization of adsorption process parameters by response surface methodology for hexavalent chromium removal from aqueous solutions using Annona reticulata Linn peel microparticles, Water Sci. Technol., 75 (2017) 2094–2107.
[21] K. Balakrishna Prabhu, M.B. Saidutta, M. Srinivas Kini, Adsorption of hexavalent chromium from aqueous medium using a new Schiff base Chitosan Derivative, Int. J. Appl. Eng. Res., 12 (2017) 4072–4082.
[22] YY.A.B. Neolaka, E.B.S. Kalla, G. Supriyanto, Suyanto, N.N.T. Puspaningsih, Adsorption of hexavalent chromium from aqueous solutions using acid activated of natural zeolite collected from ende-flores, Indonesia, Rasayan J. Chem., 10 (2017) 606–612. doi:10.7324/RJC.2017.1021710.
[23] C. Yang, Y. Ma, S. Ding, Study on factors of effecting adsorption of Cr 6+ in wastewater by bentonite, 2012 2nd Int. Conf. Consum. Electron. Commun. Networks, CECNet 2012 - Proc., (2012) 598–601.
[24] R.M. Schneider, C.F. Cavalin, M.A.S.D. Barros, C.R.G. Tavares, Adsorption of chromium ions in activated carbon, Chem. Eng. J., 132 (2007) 355–362.
[25] C. Rahel, M. Bhatnagar, Adsorption of heavy metals and phenol from aqueous solution onto fly ash as low cost adsorbent: a review, Int. J. Innov. Res. Sci., 6 (2017) 2479–2497.
[26] R.S. Bai, T.E. Abraham, Studies on chromium(VI) adsorption-desorption using immobilized fungal biomass, Bioresour. Technol., 87 (2003) 17–26.
[27] M. Dakiky, M. Khamis, A. Manassra, M. Mer'eb, Selective adsorption of chromium(VI) in industrial wastewater using low-cost abundantly available adsorbents, Adv. Environ. Res., 6 (2002) 533–540.
[28] E. Hoseinzadeh, A.R. Rahmanie, G. Asgari, G. McKay, A.R. Dehghanian, Adsorption of acid black 1 by using activated carbon prepared from scrap tires: Kinetic and equilibrium studies, J. Sci. Ind. Res. (India), 71 (2012) 682–689.
[29] E.M. Kalhori, K. Yetilmezsoy, N. Uygur, M. Zarrabi, R.M.A. Shmeis, Modeling of adsorption of toxic chromium on natural and surface modified lightweight expanded clay aggregate (LECA), Appl. Surf. Sci., 287 (2013) 428–442.
[30] J. Madejov, P. Komadel, J. Madejova, J. Madejová, Base Line studies of the clay minerals society source clays: infrared methods, Clay Clay Miner., 49 (2001) 410–432.
[31] B. Meroufel, O. Benali, M. Benyahia, M.A. Zenasni, A. Merlin, B. George, Removal of Zn (II) from aqueous solution onto kaolin by batch design, J. Water Resour. Prot., 5 (2013) 669–680.
[32] V.C. Farmer, F. Palmieri, The characterization of soil minerals by infrared spectroscopy, Soil Components, Vol. 2, Inorg. Components, (1975) 573–670.
[33] V.C. Farmer, Transverse and longitudinal crystal modes associated with OH stretching vibrations in single crystals of kaolinite and dickite, Spectrochim. Acta - Part A Mol. Biomol. Spectrosc., 56 (2000) 927–930.
[34] O. Allahdin, M. Wartel, J. Mabingui, A. Boughriet, Implication of Electrostatic forces on the adsorption capacity of a modified brick for the removal of divalent cations from water, Am. J. Anal. Chem., 6 (2015) 11–25.
[35] Y.H. Chen, F.A. Li, Kinetic study on removal of copper(II) using goethite and hematite nano-photocatalysts, J. Colloid Interface Sci., 347 (2010) 277–281.
[36] A. Tironi, M.A. Trezza, E.F. Irassar, A.N. Scian, Thermal treatment of kaolin: effect on the pozzolanic activity, Procedia Mater. Sci., 1 (2012) 343–350.
[37] A.K. Panda, B.G. Mishra, D.K. Mishra, R.K. Singh, Effect of sulphuric acid treatment on the physico-chemical characteristics of kaolin clay, Colloids Surfaces A Physicochem. Eng. Asp., 363 (2010) 98–104.
[38] C. Starbuck, V. Stiles, D. Urà, M. Carré, S. Dixon, Biomechanical responses to changes in friction on a clay court surface, J. Sci. Med. Sport., 20 (2017) 459–463.
[39] B.K. Nandi, A. Goswami, M.K. Purkait, Adsorption characteristics of brilliant green dye on kaolin, J. Hazard. Mater., 161 (2009) 387–395.
[40] B.K. Nandi, A. Goswami, M.K. Purkait, Removal of cationic dyes from aqueous solutions by kaolin: Kinetic and equilibrium studies, Appl. Clay Sci., 42 (2009) 583–590.
[41] J. Kiurski, J. Ranogajec, S. Vucetic, D. Zoric, S. Adamovic, I. Oros, J. Krstic, Fired clay with polymer addition as printing developer purifier, Appl. Clay Sci., 65–66 (2012) 48–52.
[42] N.Y. Mezenner, A. Bensmaili, Kinetics and thermodynamic study of phosphate adsorption on iron hydroxide-eggshell waste, Chem. Eng. J., 147 (2009) 87–96.
[43] S. Karaca, A. Gürses, M. Açikyildiz, M. Ejder (Korucu), Adsorption of cationic dye from aqueous solutions by activated carbon, Microporous Mesoporous Mater., 115 (2008) 376–382.
[44] M. Doğan, M. Alkan, A. Türkyilmaz, Y. Özdemir, Kinetics and mechanism of removal of methylene blue by adsorption onto perlite, J. Hazard. Mater., 109 (2004) 141–148.
[45] E. Nakkeeran, N. Saranya, M.S.G. Nandagopal, A. Santhiagu, N. Selvaraju, Hexavalent chromium removal from aqueous solutions by a novel powder, prepared from Colocasia esculenta leaves, Int. J. Phytoremediation, 5 (2013) 338–346.
[46] J.C. Santamarina, K.A. Klein, Y.H. Wang, E. Prencke, Specific surface: determination and relevance, Can. Geotech. J., 39 (2002) 233–241.
[47] E. Suganya, S. Rangabhashiyam, A.V. Lity, N. Selvaraju, Removal of hexavalent chromium from aqueous solution by a novel biosorbent Caryota urens seeds: equilibrium and kinetic studies, Desal. Water Treat., 57 (2016) 23940–23950.
[48] S. Rangabhashiyam, E. Suganya, N. Selvaraju, Packed bed column investigation on hexavalent chromium adsorption using activated carbon prepared from Swietenia Mahogani fruit shells, Desal. Water Treat., 57 (2016) 13048–13055.
[49] S. Asuha, X.G. Zhou, S. Zhao, Adsorption of methyl orange and Cr(VI) on mesoporous $TiO_2$ prepared by hydrothermal method, J. Hazard. Mater., 181 (2010) 204–210.
[50] S. Zhou, F. Liu, Q. Zhang, B.-Y. Chen, C.-J. Lin, C.-T. Chang, Preparation of polyacrylonitrile/ferrous chloride composite nanofibers by electrospinning for efficient reduction of Cr(VI), J. Nanosci. Nanotechnol., 15 (2015).

[51] A.A. Attia, S.A. Khedr, S.A. Elkholy, Adsorption of chromium ion (VI) by acid activated carbon, Brazilian J. Chem. Eng., 27 (2010) 183–193.
[52] G. Ghanizadeh, G. Asgari, A.M.S. Mohammade, M.T. Ghaneian, Kinetics and isotherm studies of hexavalent chromium adsorption from water using bone charcoal, Fresenius Environ. Bull., 21 (2012).
[53] O. Ajouyed, Evaluation of the Adsorption of hexavalent chromium on kaolinite and illite, J. Environ. Prot. (Irvine,. Calif), 2 (2011) 1347–1352.
[54] G. Asgari, A.R. Rahmani, J. Faradmal, A.M. Seid Mohammadi, Kinetic and isotherm of hexavalent chromium adsorption onto nano hydroxyapatite, J. Res. Health Sci., 12 (2012) 45–53.
[55] R. Bhatt, B. Sreedhar, P. Padmaja, Adsorption of chromium from aqueous solutions using crosslinked chitosan-diethylenetriaminepentaacetic acid, Int. J. Biol. Macromol., 74 (2015) 458–466.
[56] G. Rojas, J. Silva, J.A. Flores, A. Rodriguez, M. Ly, H. Maldonado, Adsorption of chromium onto cross-linked chitosan, Sep. Purif. Technol., 44 (2005) 31–36.
[57] G. Asgari, B. Ramavandi, L. Rasuli, M. Ahmadi, Cr (VI) adsorption from aqueous solution using a surfactant-modified Iranian zeolite: Characterization, optimization, and kinetic approach, Desal. Water Treat., 51 (2013) 6009–6020.
[58] B. Ramavandi, G. Asgari, J. Faradmal, S. Sahebi, B. Roshani, Abatement of Cr (VI) from wastewater using a new adsorbent, cantaloupe peel: Taguchi L16orthogonal array optimization, Korean J. Chem. Eng., 31 (2014) 2207–2214.
[59] S.T. Akar, Y. Yetimoglu, T. Gedikbey, Removal of chromium (VI) ions from aqueous solutions by using Turkish montmorillonite clay: effect of activation and modification, Desalination, 244 (2009) 97–108.
[60] C.H. Giles, T.H. MacEwan, S.N. Nakhwa, System of classification of solution adsorption isotherms and its use in diagnosis of adsorption of mechanisms and in measurements of specific surface area of solids, J. Chem. Soc., 10 (n.d.) 3973–3993.
[61] I. Langmuir, The constitution and fundamental properties of solids and liquids., J. Am. Chem. Soc., 39 (1917) 1848–1906.
[62] N. Ayawei, S.S. Angaye, D. Wankasi, E. Dixon Dikio, N. Ayawei, Synthesis, characterization and application of Mg/Al layered double hydroxide for the degradation of Congo Red in aqueous solution, Open J. Phys. Chem. Synth., 5 (2015) 56–70.
[63] G. McKay, M.S. Otterburn, A.G. Sweeney, The removal of colour from effluent using various adsorbents-III. Silica: Rate processes, Water Res., 14 (1980) 15–20.
[64] A. Özer, H.B. Pirinççi, The adsorption of Cd(II) ions on sulphuric acid-treated wheat bran, J. Hazard. Mater., 137 (2006) 849–855.
[65] A. Dada, A. Olalekan, A. Olatunya, O. Dada, Langmuir, Freundlich , Temkin and Dubinin – Radushkevich isotherms studies of equilibrium sorption of $Zn^{2+}$ unto phosphoric acid modified rice husk, IOSR J. Appl. Chem., 3 (2012) 38–45.
[66] M.I. Temkin, The Kinetics of Some Industrial Heterogeneous Catalytic Reactions, 1979.
[67] R.R. Krishni, K.Y. Foo, B.H. Hameed, Adsorption of methylene blue onto papaya leaves: comparison of linear and nonlinear isotherm analysis, Desal. Water Treat., 52 (2014) 6712–6719.
[68] Y.S. Ho, D.A.J. Wase, C.F. Forster, Kinetic studies of competitive heavy metal adsorption by sphagnum moss peat, Environ. Technol. (United Kingdom), 17 (1996) 71–77.
[69] Y.S. Ho, G. McKay, Pseudo-second order model for sorption processes, Process Biochem., 34 (1999) 451–465.
[70] V. Zelentsov, T. Datsko, Modelling of kinetics of fluorine adsorption onto modified diatomite, Sci. Study Res. Chem. Chem. Eng. Biotechnol. Food Ind., 18 (2017) 85–95.
[71] K. Kayalvizhi, K. Vijayaraghavan, M. Velan, Biosorption of Cr(VI) using a novel microalga Rhizoclonium hookeri: equilibrium, kinetics and thermodynamic studies, Desal. Water Treat., 56 (2015) 194–203.
[72] K. Parida, K.G. Mishra, S.K. Dash, Adsorption of toxic metal ion Cr(VI) from aqueous state by $TiO_2$-MCM-41: Equilibrium and kinetic studies, J. Hazard. Mater., 241–242 (2012) 395–403.
[73] A.B. Albadarin, A.H. Al-Muhtaseb, G.M. Walker, S.J. Allen, M.N.M. Ahmad, Retention of toxic chromium from aqueous phase by $H_3PO_4$-activated lignin: Effect of salts and desorption studies, Desalination, 274 (2011) 64–73.
[74] A.E. Ofomaja, E.I. Unuabonah, Kinetics and time-dependent Langmuir modeling of 4-nitrophenol adsorption onto Mansonia sawdust, J. Taiwan Inst. Chem. Eng., 44 (2013) 566–576.
[75] W. Liu, J. Zhang, C. Zhang, Y. Wang, Y. Li, Adsorptive removal of Cr (VI) by Fe-modified activated carbon prepared from Trapa natans husk, Chem. Eng. J., 162 (2010) 677–684.
[76] M. Ramaswamy, Synthesis, Sorption and kinetic characteristics of silica-hexacyanoferrate composites, Solvent Extr. Ion Exch., 17 (1999) 1603–1618.
[77] A.M. Donia, A.A. Atia, H. El-Boraey, D.H. Mabrouk, Uptake studies of copper(II) on glycidyl methacrylate chelating resin containing $Fe_2O_3$ particles, Sep. Purif. Technol., 49 (2006) 64–70.
[78] Z. Yavari, M. Noroozifar, Kinetic, isotherm and thermodynamic studies with linear and non-linear fitting for cadmium(II) removal by black carbon of pine cone, Water Sci. Technol., 76 (2017) 2242–2253.
[79] S. Chen, Q. Yue, B. Gao, X. Xu, Equilibrium and kinetic adsorption study of the adsorptive removal of Cr(VI) using modified wheat residue, J. Colloid Interface Sci., 349 (2010) 256–264.
[80] C.H. Weng, Y.C. Sharma, S.H. Chu, Adsorption of Cr(VI) from aqueous solutions by spent activated clay, J. Hazard. Mater., 155 (2008) 65–75.
[81] S.K. Bajpai, Removal of hexavalent chromium by adsorption onto fireclay and impregnated fireclay, Sep. Sci. Technol., 36 (2001) 399–415.
[82] N. Daneshvar, D. Salari, S. Aber, Chromium adsorption and Cr(VI) reduction to trivalent chromium in aqueous solutions by soya cake, J. Hazard. Mater., 94 (2002) 49–61.
[83] O. Ajouyed, C. Hurel, O. Ajouyed, C. Hurel, N. Marmier, Evaluation of the Adsorption of Hexavalent Chromium on Kaolinite and Illite Evaluation of the Adsorption of Hexavalent Chromium on Kaolinite and Illite, (2011). doi:10.4236/jep.2011.210155.
[84] M.E. Argun, S. Dursun, C. Ozdemir, M. Karatas, Heavy metal adsorption by modified oak sawdust: Thermodynamics and kinetics, J. Hazard. Mater., 141 (2007) 77–85.
[85] Ş.S. Bayazit, Ö. Kerkez, Hexavalent chromium adsorption on superparamagnetic multi-wall carbon nanotubes and activated carbon composites, Chem. Eng. Res. Des., 92 (2014) 2725–2733.
[86] O. Abollino, M. Aceto, M. Malandrino, C. Sarzanini, E. Mentasti, Adsorption of heavy metals on Na-montmorillonite. Effect of pH and organic substances, Water Res., 37 (2003) 1619–1627.
[87] P.K. Pandey, S.K. Sharma, S.S. Sambi, Kinetics and equilibrium study of chromium adsorption on zeolite, NaX, 7 (2010) 395–404.
[88] M. Doğan, M. Alkan, Ö. Demirbaş, Y. Özdemir, C. Özmetin, Adsorption kinetics of maxilon blue GRL onto sepiolite from aqueous solutions, Chem. Eng. J., 124 (2006) 89–101.